ADVANCED FUNCTIONAL MATERIALS
www.afm-journal.de



# Zn(II)-Protoporphyrin IX-Based Photosensitizer-Imprinted Au-Nanoparticle-Modified Electrodes for Photoelectrochemical Applications

*Tzuriel Simcha Metzger, Ran Tel-Vered, Hendrik Bauke Albada, and Itamar Willner**

**The electropolymerization of thioaniline-modified Au nanoparticles (NPs) on thioaniline monolayer-functionalized electrodes in the presence of Zn(II)-protoporphyrin IX yields bis aniline-crosslinked Au NPs matrices that include molecular imprinted sites for binding the Zn(II)-protoporphyrin IX photosensitizer. The binding of the photosensitizer yields photoelectrochemically active electrodes that produce anodic photocurrents in the presence of the electron donor benzohydroquinone. The efficient photocurrents formed in the presence of the imprinted electrode are attributed to the high-affinity binding of the photosensitizer to the imprinted sites, $K_a = 3.2 \times 10^6$ M$^{-1}$, and to the effective transport of the photoejected electrons to the bulk electrode via the bridged Au NPs matrix. Similarly, a *N*,*N*′-dialkyl-4,4′-bipyridinium-modified Zn(II)-protoporphyrin IX photosensitizer-electron acceptor dyad is imprinted in the bis aniline-crosslinked Au NPs matrix. The photocurrent generated by the imprinted matrix is approximately twofold higher as compared to the photocurrent generated by the Zn(II)-protoporphyrin IX-imprinted Au NPs matrix. The efficient photocurrents generated in the presence of the bipyridinium-modified Zn(II)-protoporphyrin IX-imprinted matrix are attributed to the effective primary charge separation of the electron–hole species in the dyad structure, followed by the effective transport of the photoejected electrons to the electrode via the bis aniline-crosslinked Au NPs matrix.**

## 1. Introduction

The construction of nanoparticle (NP)-functionalized electrodes for photoelectrochemical and solar cells applications attracted substantial research efforts in the past two decades.[1] Specifically, the assembly of 2D or 3D arrays of semiconductor NPs[2] or composites of semiconductor NPs/metal NPs[3] (or carbon nanotubes[4]) were applied to assemble photoelectrochemically active electrodes. Different methods to functionalize the electrodes with the NPs were reported, and these included the covalent attachment of the NPs to the surfaces,[5] the layer-by-layer deposition of the NPs by electrostatic interactions,[6] and the aggregation of NPs by supramolecular interactions.[7] Also, the electropolymerization of chemically modified NPs onto electrodes[8] or the bridging of NPs on electrodes by biomolecular complementary interactions, such as duplex nucleic acid bridges,[9] were used to assemble photoelectrochemically active electrodes. Besides the use of semiconductor NPs as the photoactive compounds for generating photocurrents, organic polymers,[10] or transition metal complexes,[11,12] were applied for stimulating the generation of photocurrents. In all of these systems, the primary photoexcitation of the light-active materials is followed by an electron transfer process that yields electron–hole species. The thermodynamically favored recombination of the electron–hole pair acts as a destructive path that decreases the light-to-electrical power conversion efficiencies. Different methods to facilitate charge separation and stabilize the electron–hole species against recombination were reported, including the use of hybrid NP structures,[13] NP–carbon nanotubes,[14] NP–polymers, or NP–molecular relay hybrids.[15] Also, the electrochemical crosslinking of semiconductor NPs onto electrodes by charge-carrying bis aniline units, was suggested as a means to induce charge separation and to enhance the generation of photocurrents.[16] In addition, supramolecular assemblies consisting of photoactive transition metal complexes, e.g., Zn(II)-porphyrins, Zn(II)-phthalocyanines, or Ru(II)-polypyridine complexes linked to molecular charge carriers or nanoparticles, were applied to improve charge separation and to increase the photocurrent efficiencies.[17]

Imprinting of specific binding sites into organic or inorganic polymer matrices has been a subject of extensive research in the past several decades.[18] Specifically, the imprinting of selective binding sites in crosslinked metallic NPs has been a subject of extensive research in recent years. The electrochemical crosslinking of redox monolayer-functionalized metal NPs, e.g., thioaniline-modified Au NPs, in the presence of a substrate (or a structural analog), exhibiting supramolecular binding affinities to the NP's capping monolayer, yielded a crosslinked metal NPs matrix that bound the respective substrates (or their structural analog) by affinity interactions. The subsequent rinsing off of the substrate (or structural analog) resulted in the formation of a metal NPs matrix (e.g., bis aniline-bridged Au NPs)

T. S. Metzger, Dr. R. Tel-Vered, Dr. H. B. Albada, Prof. I. Willner
Institute of Chemistry
The Hebrew University of Jerusalem
Jerusalem 91904, Israel
E-mail: willnea@vms.huji.ac.il

DOI: 10.1002/adfm.201502801

that included high-affinity and selective imprinted sites for the binding of the respective substrates. Selective imprinted sites for the binding of explosives,[19] saccharides,[20] amino acids and peptides,[21] antibiotics,[22] and metal ions[23] were reported, and the imprinted Au NPs matrices were used for the development of sensitive sensors, for the assembly of electrochemically triggered NP sponges for the controlled uptake and release of substrates,[24] and for the construction of functional interfaces of electrically triggered wettability properties.[25] Also, the electrochemical crosslinking of thioaniline-modified Au NPs with thioaniline-functionalized semiconductor quantum dots (e.g., CdS),[3a] or thioaniline-modified native photosystems,[26] yielded photoelectrochemically active electrodes for the generation of photocurrents.

In the present study, we address the effects of imprinting of molecular recognition sites for Zn(II)-protoporphyrin IX (**1**), in bis aniline-crosslinked Au NPs matrices on the photosensitized generation of photocurrents. We demonstrate that the association of the Zn(II)-protoporphyrin IX photosensitizer with the imprinted sites significantly increases the photocurrent generated by the electrode as compared to a nonimprinted bis aniline-crosslinked Au NPs system. We also show that the imprinted electrode is regenerable and allows the extraction of the photosensitizer and its reloading. We further demonstrate the imprinting of a bis-bipyridinium-Zn(II)-protoporphyrin IX dyad structure in the bis aniline-crosslinked Au NPs assembly. Substantially higher photocurrents are generated by the dyad assembly as compared to the Zn(II)-protoporphyrin IX system lacking the bipyridinium electron acceptor units. The enhanced photocurrents in the presence of the photosensitizer dyad structure are attributed to the improved charge separation of the photogenerated electron–hole species in the system.

## 2. Results and Discussion

**Figure 1**A depicts the method to assemble the imprinted Zn(II)-protoporphyrin IX (Zn(II)-PP-IX) (**1**), matrix. The imprinting paradigm is based on electrostatic interactions between the Zn(II)-PP-IX carboxylated photosensitizer and the bis anilinium bridging units generated upon crosslinking the Au NPs. A Au electrode was modified with a monolayer of electropolymerizable thioaniline (**2**) units. Electropolymerization of the (**2**)-modified Au surface in the presence of Au NPs (diameter ≈ 4.5 nm) modified with (**2**), and with mercaptoethane sulfonic acid (**3**) units as stabilizing units, and in the presence of Zn(II)-PP-IX, yielded the (**1**)-imprinted bis aniline-bridged Au NPs matrix. Subsequently, the Zn(II)-PP-IX photosensitizer was eliminated from the imprinted sites, through extensive rinsing with a sodium acetate buffer solution. Similarly, a nonimprinted Au NPs matrix was prepared on a Au surface by the electropolymerization of the (**2**)/(**3**)-capped Au NPs on a (**2**)-modified Au surface in the absence of Zn(II)-PP-IX, and under similar electropolymerization conditions. The bis aniline

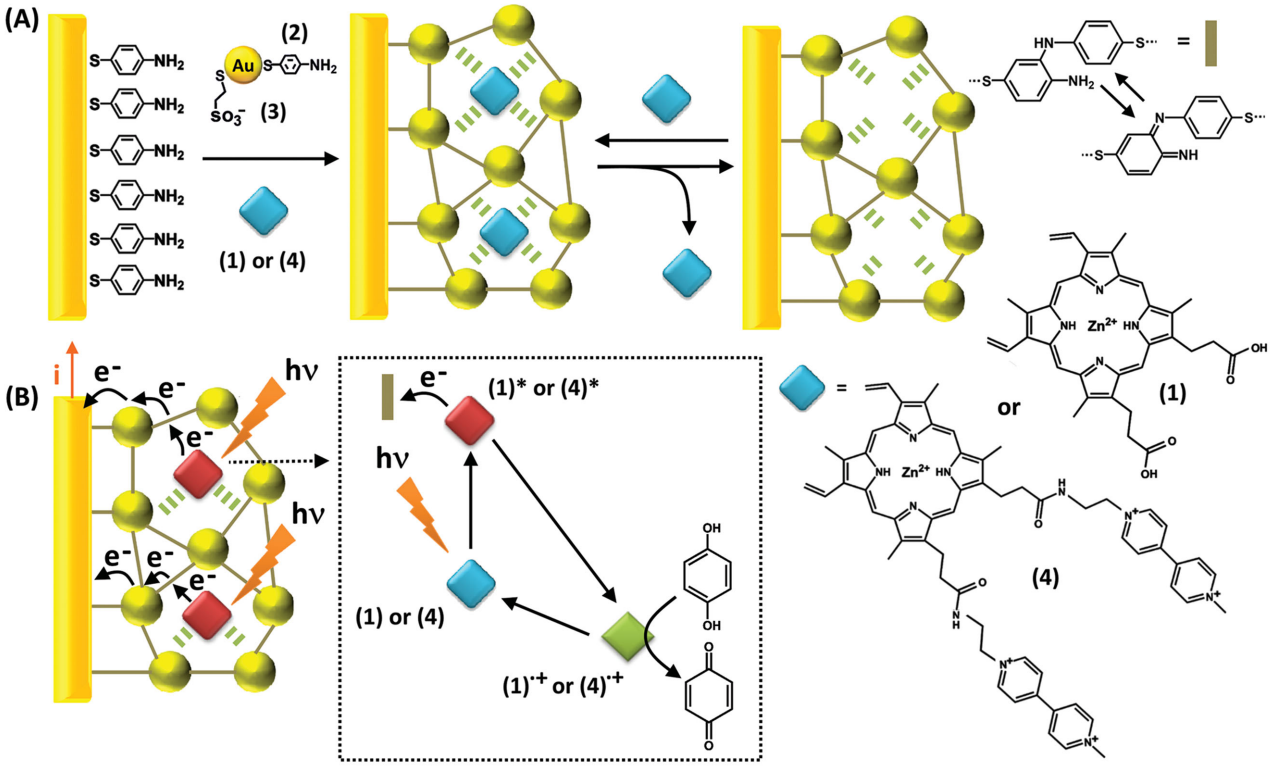


**Figure 1.** A) Molecular imprinting of Zn(II)-PP-IX or Zn(II)-PP-$V^{2+}$ photosensitizer units in bis aniline-crosslinked Au NP matrices for the generation of photocurrents. B) The electron transfer pathway for the generation of anodic photocurrents upon the illumination of the Zn(II)-PP-IX- or Zn(II)-PP-$V^{2+}$-imprinted bis aniline-crosslinked Au NPs matrices in the presence of a benzohydroquinone electron donor. Blue, red, and green squares correspond to the ground-state photosensitizers, photoexcited photosensitizers, and oxidized photosensitizers, respectively.

crosslinking units of the imprinted or nonimprinted Au NP matrices exhibit quasi-reversible redox features, $E^{o'}$ = 0.05 V versus a KCl-saturated calomel electrode (SCE) at pH = 7.0. Coulometric analysis of the redox waves associated with the imprinted and nonimprinted matrices demonstrated less than 8% variation, and a similar content of crosslinked Au NPs, $9.5 \pm 0.6 \times 10^{13}$ NPs cm$^{-2}$, was evaluated for both matrices using quartz crystal microbalance (QCM) measurements. Also, the atomic force microscopy (AFM) imaging of the electropolymerized films indicated rough surface patterns with spikes-shaped nanostructures reaching heights of up to ≈80 nm (Figure S1, Supporting Information).

In the next step, the imprinted as well as the nonimprinted Au NPs matrices were subjected, for 15 min to Zn(II)-PP-IX, before measuring the photocurrents generated by the systems. This time-interval leads to the saturation of the imprinted sites with Zn(II)-PP-IX. Figure 1B outlines the mechanism for the generation of photocurrents by the (**1**)-imprinted Au NPs matrix in the presence of Zn(II)-PP-IX, as a photosensitizer, and benzohydroquinone, as an electron donor. Photoexcitation of the Zn(II)-PP-IX results in the ejection of electrons to the Au NPs or to the bridging units (depending on the bias potential applied on the electrode, vide infra) and their transport to the bulk electrode. The reduction of the oxidized photosensitizer, Zn(II)-PP-IX$^{+\cdot}$ by the benzohydroquinone regenerates the photosensitizer while oxidizing the hydroquinone to benzoquinone, thus leading to a steady-state photocurrent. **Figure 2**A depicts the photocurrent action spectra

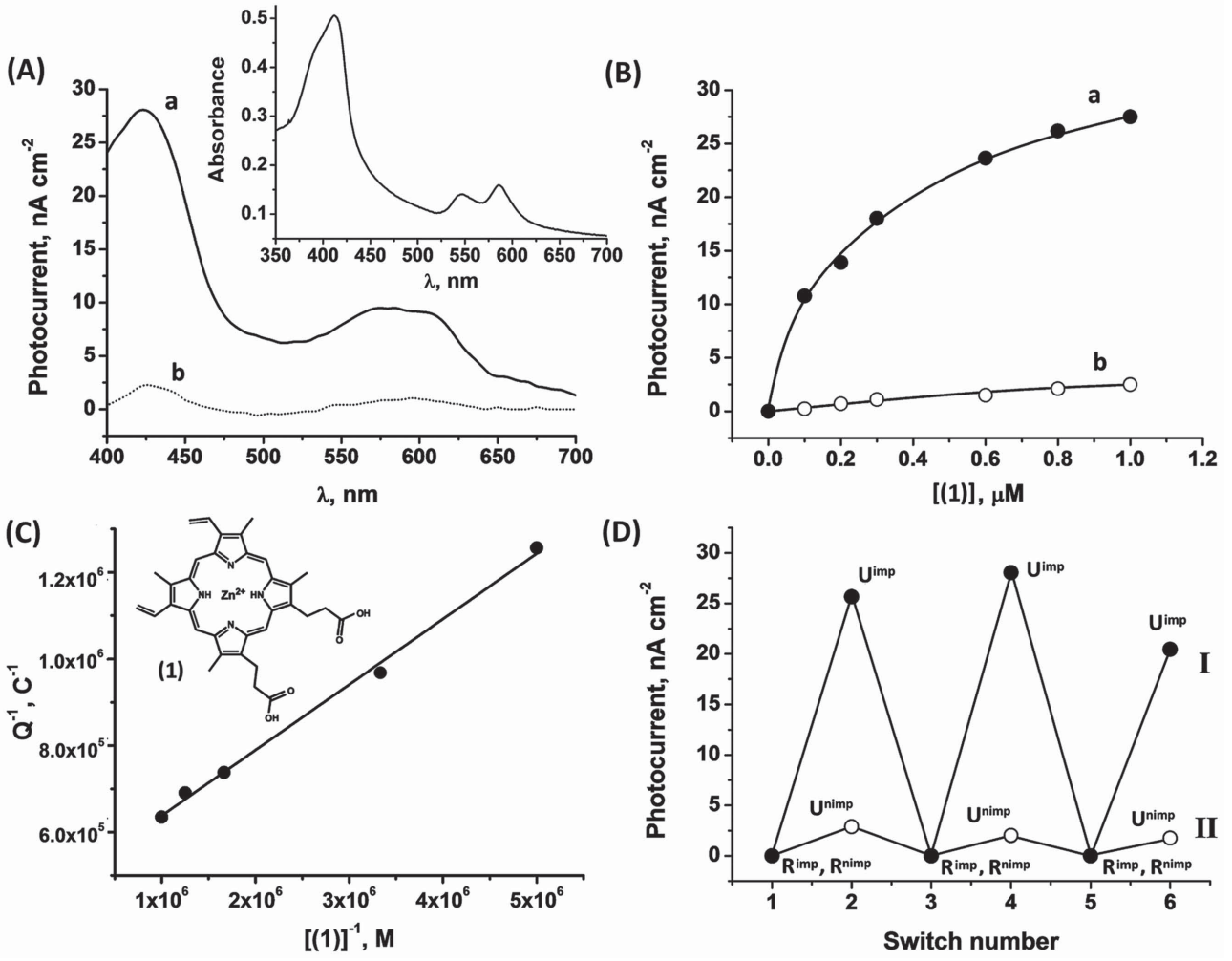


**Figure 2.** A) Photocurrent action spectra corresponding to the illumination of a) he Zn(II)-PP-IX-imprinted bis aniline-crosslinked Au NPs matrix and b) the nonimprinted bis aniline-crosslinked Au NPs matrix. Inset: UV–vis absorbance of Zn(II)-PP-IX, $1 \times 10^{-6}$ M, in a 1:1 (v/v) water:ethanol solution. B) Dependence of the photocurrent, at $\lambda = 425$ nm, on the external concentration of Zn(II)-PP-IX. Measurement were performed on a) the Zn(II)-PP-IX-imprinted matrix and b) the nonimprinted matrix. C) Coulometric analysis of the photocurrents measured for the Zn(II)-PP-IX-imprinted electrode upon the interaction of the electrode with different bulk concentrations of Zn(II)-PP-IX. D) Photocurrents generated upon the repetitive cyclic uptake (U) and release (R) of the Zn(II)-PP-IX photosensitizer by and from I) the Zn(II)-PP-IX-imprinted and II) the nonimprinted bis aniline-crosslinked Au NP electrodes. The uptake of the photosensitizer was performed by immersing the electrodes for 20 min in a 4-(2-hydroxyethyl)-1-piperazine ethane sulfonuc acid (HEPES) buffer solution (0.1 M, pH = 7.2) containing Zn(II)-PP-IX, $1 \times 10^{-6}$ M. The release of Zn(II)-PP-IX was performed by interacting the electrodes for 6 h with a sodium acetate buffer ($30 \times 10^{-3}$ M, pH = 4.5). All photocurrent measurements were performed in a HEPES buffer solution (0.1 M, pH = 7.2) containing Zn(II)-PP-IX, $1 \times 10^{-6}$ M, and benzohydroquinone, $10 \times 10^{-3}$ M. Photocurrents were measured at $\lambda = 425$ nm.

generated by the Zn(II)-PP-IX, (**1**)-imprinted matrix-modified electrode, in the presence of Zn(II)-PP-IX, $1 \times 10^{-6}$ M, and benzohydroquinone, $10 \times 10^{-3}$ M, curve (a). For comparison, the photocurrent generated at the same concentrations of Zn(II)-PP-IX/hydroquinone in the presence of the nonimprinted Au NPs matrix is depicted in Figure 2A, curve (b). Evidently, the photocurrent generated by the imprinted matrix is 11-fold higher than in the presence of the nonimprinted matrix. Control experiments reveal that upon exclusion of the hydroquinone, only trace photocurrents are formed, implying that the presence of the hydroquinone electron donor, is essential to yield the photocurrent. Figure 2A, inset, shows the absorption spectrum of Zn(II)-PP-IX in solution. Evidently, the photocurrent action spectrum correlates with the absorbance features of the photosensitizer, implying that, indeed, the photocurrent originates from the photoexcitation of Zn(II)-PP-IX. The quantum yield for the photocurrent generation was estimated to be ≈0.2%.

The amount of the Zn(II)-PP-IX bound to the imprinted Au NPs matrix is anticipated to control the magnitude of the resulting photocurrent. Figure 2B, curve (a), shows the photocurrents generated by the (**1**)-imprinted Au NPs-modified electrode in the presence of variable concentrations of Zn(II)-PP-IX. As the bulk concentration of Zn(II)-PP-IX increases, the resulting photocurrents are intensified, and they level off to a saturation value at a concentration of $1 \times 10^{-6}$ M. At higher bulk concentrations of Zn(II)-PP-IX, the intensity of the photocurrents decreases due to a light filtering effect by the high absorbance of the photosensitizer in solution. These results are consistent with the equilibrated binding of Zn(II)-PP-IX to the imprinted sites. As the bulk concentration of Zn(II)-PP-IX increases, the occupation of the imprinted sites is higher, and it reaches a saturation coverage upon occupying all sites, resulting in the saturation of the photocurrents. Assuming that the photocurrent intensities follow the binding features of Zn(II)-PP-IX to the imprinted sites, we analyzed the curve depicted in Figure 2B in terms of the Langmuir isotherm theory, Figure 2C, see the Supporting Information. Accordingly, we estimate the association constant of Zn(II)-PP-IX to the imprinted sites to be $K_a = 3.2 \times 10^6$ M$^{-1}$, and the surface coverage of imprinted sites corresponds to $2.1 \times 10^{-11}$ mol cm$^{-2}$.

The reversible uptake and release of the Zn(II)-PP-IX photosensitizer units from the imprinted matrix are demonstrated in Figure 2D. The regeneration of the active imprinted sites through the cyclic washing off of the Zn(II)-PP-IX units and their reloading to yield the active photoelectrochemical electrodes imply that the imprinted sites exhibit structural rigidity to bind the photosensitizer units. Furthermore, in all of the experiments comparing the (**1**)-imprinted Au NPs electrode to the nonimprinted matrix, substantially higher photocurrents are observed with the imprinted electrodes. The low photocurrent values observed in the presence of the nonimprinted Au NPs matrix are attributed to the low-affinity binding of Zn(II)-PP-IX to the bis aniline-crosslinked Au NPs matrix via electrostatic and/or $\pi$–$\pi$ interactions.

The system consisting of the imprinted Zn(II)-PP-IX photosensitizer includes two redox-active components: the bis aniline crosslinking units and the benzohydroquinone units acting as an electron donor. The redox bridges undergo quasi-reversible transitions between the bis aniline and quinoid states, **Figure 3**A. At $E > 0.0$ V versus SCE, the bridges exist in the quinoid structure, whereas at $E \leq 0.0$ V, the bridges exist in the reduced bis aniline state. The second redox-active unit corresponds to the hydroquinone component that reveals, in the presence of imprinted Au NPs matrix, the quasi-reversible redox wave shown in Figure 3B. At $E > 0.1$ V, the solubilized hydroquinone units are oxidized to the benzoquinone state, while at $E < 0.1$ V, they exist in the reduced hydroquinone configuration. Accordingly, one may expect that upon changing the bias potential on the electrode, the photocurrents generated by the system could be controlled. Figure 3C depicts the photocurrent intensities generated by the Zn(II)-PP-IX-imprinted Au NPs electrode upon biasing the potential on the electrode. The system generates a peak anodic photocurrent of ≈70 nA cm$^{-2}$ at approximately $E = 0.05$ V versus SCE. Shifting the potential to more positive values than that results in a decrease in the anodic photocurrent, while shifting the potential to values higher than $E > 0.15$ V, leads to a sharp transition to cathodic photocurrents (e.g., at $E = 0.2$ V, the cathodic photocurrent corresponds to ≈250 nA cm$^{-2}$). The observed potential-controlled photocurrents and the transitions from anodic to cathodic photocurrents are rationalized in terms of the redox states of the components involved in the photocurrent generation. At $E = 0.05$ V, the quinoid electron acceptor units associated with the crosslinking bridges allow the transport of the Zn(II)-PP-IX photoexcited electrons through the Au NPs to the base Au surface. Under this potential, most of the benzohydroquinone units retain their reduced electron donor state. Upon illumination, the reduction of the resulting oxidized photosensitizer, Zn(II)-PP-IX$^{\cdot+}$ by the benzohydroquinone regenerates the photosensitizer, with the concomitant transfer of the electrons trapped by the bis aniline quinoid bridges to the electrode, yielding the steady-state anodic photocurrent. At potentials $E > 0.1$ V, and particularly at $E > 0.15$ V, the hydroquinone units solubilized in the electrolyte solution are oxidized to benzoquinone, allowing its sole existence at the electrode/electrolyte interface. The high concentration of the benzoquinone acceptor units at the electrode surface results in the effective quenching of the photoexcited Zn(II)-PP-IX photosensitizer and the reduction of the Zn(II)-PP-IX$^{\cdot+}$ species by electrons supplied by the electrode lead, then, to the formation of high cathodic photocurrents. Interestingly, biasing the potential of the electrode below $E < 0.05$ V results in a decrease in the photocurrent intensity which is attributed to the electrochemical reduction of the quinoid bridges, a process that depletes the electron acceptor bridging units in the Au NPs. The ON/OFF photoswitchable generation of the peak anodic photocurrents upon biasing the Zn(II)-PP-IX-imprinted and nonimprinted matrices at $E = 0.05$ V are depicted in Figure 3D. Evidently, the comparison between the light-triggered photocurrents by the two electrodes reveals that the imprinting procedure is essential for the concentration of the photosensitizer units at the surface, thus leading to the enhanced observable photocurrent values.

The successful generation of high-affinity molecular-imprinted sites for Zn(II)-PP-IX in the bis aniline-crosslinked Au NPs matrix, and the enhanced photocurrents observed upon binding the photosensitizer Zn(II)-PP-IX to the imprinted

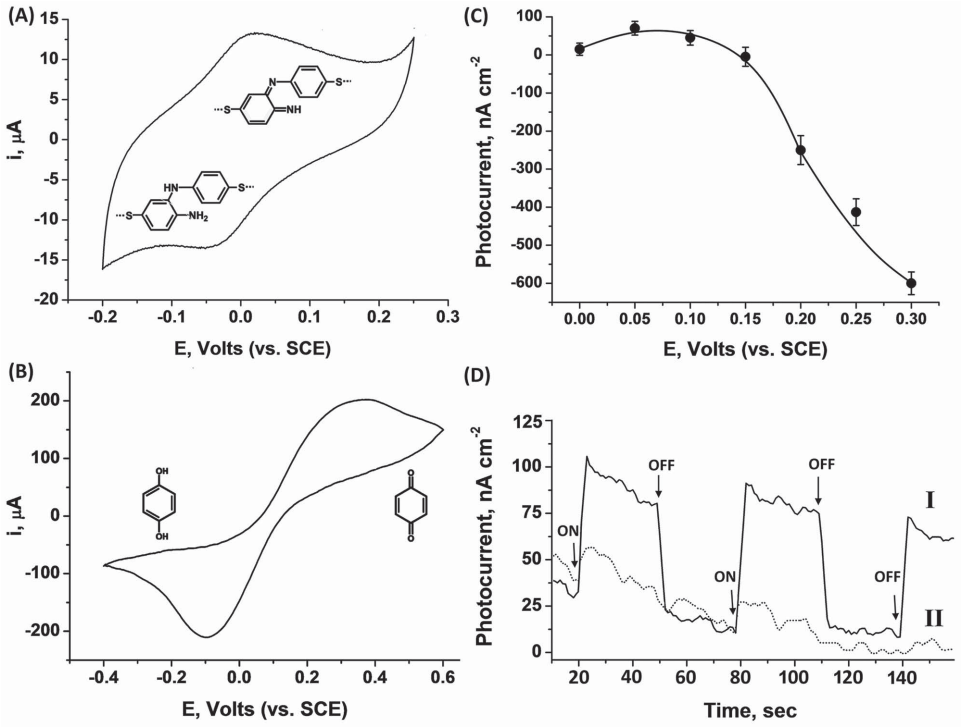


**Figure 3.** A) Cyclic voltammogram showing the redox wave of the bis aniline units associated with the crosslinked Au NPs matrix. B) Cyclic voltammogram corresponding to the redox wave of benzohydroquinone, $10 \times 10^{-3}$ M, dissolved in the electrolyte solution, in the presence of the imprinted bis aniline-crosslinked Au NPs matrix. Measurements in (A) and (B) were performed in a HEPES buffer (0.1 M, pH = 7.2). Scan rate: 100 mV $s^{-1}$. C) Potential-dependent photocurrent values corresponding to the application of variable potentials on the Zn(II)-PP-IX-imprinted bis aniline-crosslinked Au NPs electrode. Measurements were performed in a HEPES buffer solution (0.1 M, pH = 7.2) containing Zn(II)-PP-IX, $1 \times 10^{-6}$ M, and benzohydroquinone, $10 \times 10^{-3}$ M. Photocurrents were measured at $\lambda = 425$ nm. Error bars correspond to a set of $N = 4$ measurements. D) Time-dependent switchable photocurrents generated by I) the Zn(II)-PP-IX-imprinted and II) the nonimprinted bis aniline-crosslinked Au NPs electrodes, upon the application of cyclic ON/OFF illumination (indicated by arrows) at $\lambda = 425$ nm. Bias potential applied on the electrode $E = 0.05$ V versus SCE. All measurements were performed in a HEPES buffer solution (0.1 M, pH = 7.2) containing Zn(II)-PP-IX, $1 \times 10^{-6}$ M, and benzohydroquinone, $10 \times 10^{-3}$ M.

sites, suggest that by the appropriate structural modification of the photosensitizer, the resulting photocurrents could be improved. Numerous studies have implemented photosensitizer-electron acceptor dyads,[27] triads,[28] tetrads,[29] or electron donor/photosensitizer/electron acceptor triads,[30] as supramolecular nanostructures that mimic the electron transfer reactions of the native photosynthetic apparatus. The stepwise electron transfer processes in these systems lead to the spatial separation of the photogenerated reduced and oxidized species, thus retarding the destructive back electron transfer reactions, and enhancing the yields of photocurrent efficiencies. Accordingly, the imprinting of a photosensitizer-electron acceptor dyad structure in the bis aniline-crosslinked Au NP matrices could lead to functional electrodes exhibiting enhanced photocurrent generation efficiencies. Previous studies have implemented the bis-*N*-methyl-4,4′-bipyridinium-Zn(II)-protoporphyrin-IX, (**4**), Zn(II)-PP-$V^{2+}$, as a functional dyad for the bridging of layered Au NP structures and generating photocurrents.[27e,f] Also, *N*,*N*′-4,4′-dialkylbipyridinium salts were imprinted in bis aniline-crosslinked Au NPs using donor–acceptor interactions between the bis aniline donor and the bipyridinium acceptor units as the imprinting paradigm.[24b] Accordingly, the (**2**)/(**3**)-capped Au NPs were electropolymerized on the (**2**) monolayer-modified electrode in the presence of Zn(II)-PP-$V^{2+}$ (**4**), and following the rinsing off of the photoactive dyad, a Zn(II)-PP-$V^{2+}$-imprinted Au NPs matrix was formed (Figure 1). The photocurrents generated by the Zn(II)-PP-$V^{2+}$-imprinted Au NPs matrix in the presence of variable bulk concentrations of Zn(II)-PP-$V^{2+}$ are depicted in **Figure 4**A. As the bulk concentration of Zn(II)-PP-$V^{2+}$ increases, the resulting photocurrents are intensified, consistent with the increased occupation of the binding sites by the Zn(II)-PP-$V^{2+}$ photosensitizer units. Assuming that the resulting photocurrents originate from the binding of the photosensitizer (**4**) to the imprinted sites, and by applying the Langmuir binding model, we evaluated the association constant of Zn(II)-PP-$V^{2+}$ with the imprinted sites to be $6.7 \times 10^6$ $M^{-1}$, and the coverage of imprinted binding sites was estimated to be $3.7 \times 10^{-11}$ mol $cm^{-2}$, a value which showed a good agreement with the coulometric analysis of the bound Zn(II)-PP-$V^{2+}$. Figure 4B shows the cyclic voltammograms corresponding to the bipyridinium units of the Zn(II)-PP-$V^{2+}$ dyad associated with the imprinted sites, as a function of the sweep rates. The peak currents reveal a linear relationship to the sweep rates, Figure 4B, inset, consistent with the surface confinement of the Zn(II)-PP-$V^{2+}$ on the imprinted Au NPs matrix.

The photocurrent action spectrum generated by the Zn(II)-PP-$V^{2+}$-imprinted Au NPs matrix in the presence of the dyad,

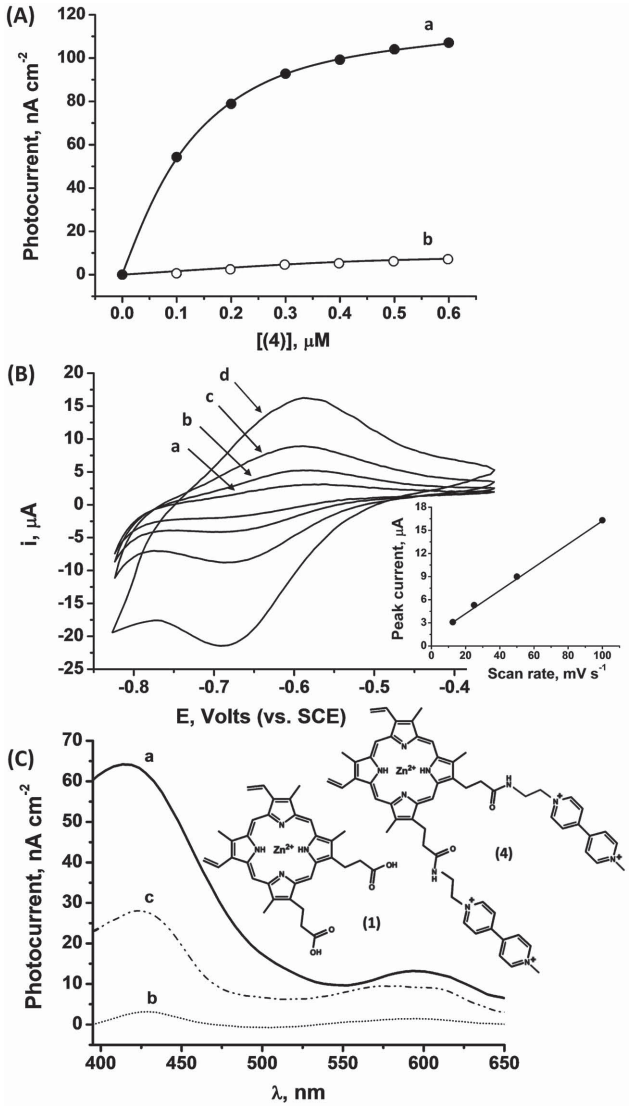


**Figure 4.** A) Dependence of the photocurrent, at $\lambda$ = 425 nm, on the external concentration of Zn(II)-PP-$V^{2+}$. Measurement were performed on a) the Zn(II)-PP-$V^{2+}$-imprinted matrix and b) the nonimprinted matrix. B) Cyclic voltammograms corresponding to the Zn(II)-PP-$V^{2+}$-imprinted matrix in the presence of $0.6 \times 10^{-6}$ M Zn(II)-PP-$V^{2+}$ at variable scan rates: a) 10, b) 25, c) 50, and d) 100 mV $s^{-1}$. Inset: Calibration curve showing the dependence of the peak anodic current, at $E = -0.6$ V versus SCE, on the applied scan rate. C) Photocurrent action spectra corresponding to a) the Zn(II)-PP-$V^{2+}$-imprinted matrix in the presence of Zn(II)-PP-$V^{2+}$, $0.6 \times 10^{-6}$ M, b) the nonimprinted matrix in the presence of Zn(II)-PP-$V^{2+}$, $0.6 \times 10^{-6}$ M, and c) the Zn(II)-PP-IX-imprinted matrix in the presence of Zn(II)-PP-IX, $1 \times 10^{-6}$ M. For comparison, the photocurrent in curve (a) was normalized to the surface coverage of Zn(II)-PP-IX in curve (c). In all systems, benzohydroquinone, $10 \times 10^{-3}$ M, was used as an electron donor.

normalized to the surface coverage of the Zn(II)-PP-IX units in the Zn(II)-PP-IX-imprinted Au NPs matrix, and under conditions where the imprinted sites are saturated, is depicted in Figure 4C, curve (a). For comparison, the photocurrent action spectrum generated by the nonimprinted bis aniline-crosslinked Au NPs matrix under similar conditions, is shown in Figure 4C, curve (b). Evidently, the imprinted Au NPs system reveals a ≈20-fold increase in the photocurrent as compared to the nonimprinted matrix. This result demonstrates that the origin for the high photocurrents is the concentration of the photosensitizer-electron acceptor Zn(II)-PP-$V^{2+}$ dyad on the electrode by the imprinted sites. Under these conditions, a photocurrent quantum yield of 0.5% was evaluated for the dyad-imprinted Au NPs matrix. Figure 4C, curve (c), depicts the photocurrent action spectrum of the Zn(II)-PP-IX-imprinted Au NPs matrix in the presence of Zn(II)-PP-IX (lacking the attached bipyridinium units) under the conditions where the imprinted sites are saturated. Clearly, for a similar surface coverage of the photosensitizer units, the photocurrent generated by the Zn(II)-PP-$V^{2+}$-imprinted matrix is more than twofold higher as compared to the Zn(II)-PP-IX-imprinted electrode. This enhancement is attributed to the more effective charge separation in the Zn(II)-PP-$V^{2+}$ system. Upon illumination, the primary charge separation in the dyad proceeds to yield Zn(II)-$PP^{\cdot+}$-$V^{\cdot+}$. The subsequent reduction of the quinoid bridging units by the $V^{\cdot+}$ entities, followed by the reduction of the photogenerated holes by the solubilized hydroquinone electron donor, allow the subsequent transport of the electrons to the base electrode surface, leading to the effective generation of the anodic photocurrent observed.

## 3. Conclusion

The present study has demonstrated the successful generation of imprinted binding sites for photosensitizer units in bis aniline-crosslinked Au NP matrices associated with electrodes. The imprinting paradigm is based on electrostatic and/or donor–acceptor interactions between the imprinted photosensitizer units and the bis aniline units bridging the Au NPs, which are formed upon the electropolymerization of thioaniline-functionalized Au NPs. Two photosensitizers, Zn(II)-protoporphyrin IX, Zn-PP-IX, and bis-bipyridinium-modified Zn(II)-protoporphyrin IX, Zn(II)-PP-IX-$V^{2+}$, were imprinted in the Au NP matrices. Enhanced anodic photocurrents were demonstrated upon subjecting the Zn(II)-PP-IX- or Zn(II)-PP-IX-$V^{2+}$-imprinted electrodes to the respective photosensitizers and in the presence of benzohydroquinone as an electron donor, as compared to the photocurrents generated by the nonimprinted bis aniline-crosslinked Au NPs matrix under similar conditions. The enhanced photocurrents observed for the imprinted matrices were attributed to (i) the effective loading of the electrodes with the photosensitizers by means of the imprinted sites and (ii) the effective transport of the photoejected electrons to the electrode supports by means of the bis aniline bridging units. We further demonstrate that the bipyridinium-functionalized Zn(II)-PP-IX-$V^{2+}$ dyad-imprinted system reveals intensified photocurrents as compared to the Zn(II)-PP-IX-imprinted matrix. These enhanced photocurrents were attributed to the primary charge separation of the electron–hole species in the dyad structure. In view of these results, the concentration of chromophores at electrode surfaces by means of molecularly engineered dyad, triads, or even tetrads, could become a general principle for tailoring dye-photosensitized photoelectrochemical cells of improved efficiencies.

## 4. Experimental Section

*Materials*: Synthesis of bis-*N*-methyl-4,4′-bipyridinium-Zn(II)-protoporphyrin-IX: The Zn(II)-PP-$V^{2+}$ photosensitizer was synthesized according to a previously reported procedure.[27e]

Au NPs Synthesis: Au nanoparticles capped with 2-mercaptoethane sulfonic acid and *p*-aminothiophenol were prepared by mixing a 100 mL methanol solution containing 197 mg $HAuCl_4$ with a 5 mL methanol solution containing 42 mg mercaptoethane sulfonate and 8 mg *p*-aminothiophenol. The two solutions were stirred in the presence of 2.5 mL glacial acetic acid in an ice bath for 30 min. Subsequently, 7.5 mL aqueous solution of 1 M sodium borhydride, $NaBH_4$, was added dropwise to the solution, resulting in a dark color, associated with the presence of the Au NPs. The solution was stirred for 1 additional hour in an ice bath and then for 14 h at room temperature. The particles were successively centrifuged and washed (twice in each solvent) with methanol, ethanol, and diethyl ether. The average size of the NPs was estimated by transmission electron microscopy (TEM) to be $3.6 \pm 0.6$ nm.

*Modification of the Electrodes*: Thioaniline-functionalized electrodes were prepared by immersing Au-coated glass slides for 3 h in an ethanolic solution containing *p*-aminothiophenol, $10 \times 10^{-3}$ M. In order to prepare the bis aniline-crosslinked Au NPs composites, 2.7 mg $mL^{-1}$ of the functionalized Au NPs, dissolved in a HEPES buffer solution (0.1 M, pH = 7.2), were electropolymerized on the *p*-aminothiophenol-modified Au electrodes in the presence of Zn(II)-PP-IX or Zn(II)-PP-$V^{2+}$, $2.4 \times 10^{-3}$ M, imprint guest molecules (for the preparation of the imprinted matrices), or in the absence of the guest molecules (for the preparation of the nonimprinted matrices). Electropolymerization was performed by the application of 80 potential cycles between –0.2 and 1.1 V versus KCl-saturated calomel electrode, SCE, at a scan rate of 100 mV $s^{-1}$. The resulting films were, then, washed with the background buffer solution to exclude any residual monomer from the electrode. The extraction of the porphyrin sensitizer molecules from the film was carried out by immersing the electrodes in a sodium acetate buffer solution ($30 \times 10^{-3}$ M, pH = 4.5) for 6 h under stirring conditions, and thoroughly washing with a HEPES buffer solution (0.1 M, pH = 7.2). The full removal of the porphyrin molecules from the electropolymerized films was verified by periodically monitoring the decrease in the photocurrents and the voltammetric response of the Zn(II)-PP-$V^{2+}$-imprinted electrode.

*Instrumentation and Methods*: Photoelectrochemical measurements were performed using a home-built system that included a Xe lamp (Oriel, model 6258, $P = 300$ W), a monochromator (Oriel, model 74000, 2 nm resolution), and a chopper (Oriel, model 76994). The electrical output from the cell was sampled by a lock-in amplifier (Stanford Research, model SR 830 DSP). The shutter chopping frequency was controlled by a Stanford Research pulse/delay generator, model DE535. The effective illumination area of all modified electrodes was 0.2 $cm^2$. The photogenerated currents were measured between the modified working electrodes and a Pt counter electrode, while constantly purging the electrolyte with Ar. The time-dependent photocurrent experiments employed an Autolab potentiostat (ECO Chemie, The Netherlands) driven by general purpose electrochemical system (GPES) software which was coupled to the photoelectrochemical apparatus, allowing the measurement of the photocurrents upon the application of different external potentials on the modified surfaces. In these experiments, a Ag wire ($d = 0.5$ mm), and a Pt sheet, were used as the reference and counter electrodes, respectively, and the values reported represent the difference between the currents measured under illumination and dark. QCM measurements were performed using a home-built instrument linked to a frequency analyzer (Fluke) using Au-quartz crystals (AT-cut 10 MHz). AFM images were captured in a tapping mode on a Digital Nanoscope IV instrument employing Si cantilevers (NSC15/AIBS, MicroMash, Estonia, resonance frequency order of 320 kHz). Absorption spectra were recorded using a UV–vis spectrophotometer (Shimadzu UV2401PC).

The internal photocurrent quantum yield corresponding to the number of electrons generated/number of photons absorbed was calculated as follows. The intensities of the transmitted and reflected light were subtracted from the intensity of the incident light to yield the absorbed light intensity, *P*. The internal quantum yield was, then, evaluated using Equation (1).

$$\phi = hcI/\lambda eP \quad (1)$$

where *I* is the measured photocurrent, *h* is Planck's constant, *c* is the vacuum velocity of light, $\lambda$ is the selected wavelength of light, and *e* is the charge of an electron.

## Supporting Information

Supporting Information is available from the Wiley Online Library or from the author.

## Acknowledgements

This research was supported by the NanoSensoMach ERC Advanced Grant No. 267574 under the EC FP7/2007-2013 program.

Received: July 8, 2015
Revised: August 23, 2015
Published online: September 24, 2015

[1] a) A. Hegfeldt, G. Boschloo, L. Sun, L. Kloo, H. Petersson, *Chem. Soc. Rev.* **2010**, *110*, 6595; b) P. V. Kamat, *Chem. Rev.* **1993**, *120*, 7847; c) B. O'Regan, J. R. Durrant, *Acc. Chem. Res.* **2009**, *42*, 1799; d) A. Hagfeldt, M. Graetzel, *Chem. Rev.* **1995**, *95*, 49.

[2] a) T. Cassagneau, T. E. Mallouk, J. H. J. Fendler, *J. Am. Chem. Soc.* **1998**, *120*, 7848; b) A. N. Shipway, E. Katz, I. Willner, *Chem. Phys. Chem.* **2000**, *1*, 18; c) J. Poppe, S. G. Hickey, A. Eychmueller, *J. Phys. Chem. C* **2014**, *118*, 17123.

[3] a) H. B. Yildiz, R. Tel-Vered, I. Willner, *Adv. Funct. Mater.* **2008**, *18*, 3497; b) Y. Takahashi, S. Yamada, T. Tatsumab, *Electrochemistry* **2014**, *82*, 726; c) P. Thiyagarajan, H. Ahn, J. Lee, J. Yoon, J. Jang, *Small* **2013**, *9*, 2341; d) F. Xiao, F. Wang, X. Fu, Y. Zheng, *J. Mater Chem.* **2012**, *22*, 2868.

[4] a) S. Zhang, H. Niu, Y. Lan, C. Cheng, J. Xu, X. Wang, *J. Phys. Chem. C* **2011**, *115*, 22025; b) J. Park, W. Choi, *J. Phys. Chem. C* **2009**, *113*, 20974; c) O. Ovits, R. Tel-Vered, I. Baravik, O. I. Wilner, I. Willner, *J. Mater. Chem.* **2009**, *19*, 7650.

[5] a) M. Jung, M. Chu, *Nanoscale* **2014**, *6*, 9241; b) L. Li, X. Yang, J. Gao, H. Tian, J. Zhao, A. Hagfeldt, L. Sun, *J. Am. Chem. Soc.* **2011**, *133*, 8458; c) A. N. Shipway, I. Willner, *Chem. Commun.* **2001**, 2035.

[6] a) T. Kameyama, K. Okazaki, K. Takagi, T. Torimoto, *PhysChemChemPhys* **2009**, *11*, 5369; b) M. Hojeij, B. Su, S. Tan, G. Meriguet, H. H. Girault, *ACS Nano* **2008**, *2*, 984; c) A. N. Shipway, M. Lahav, R. Blonder, I. Willner, *Chem. Mater.* **1999**, *11*, 13; d) R. Blonder, L. Sheeney-Haj-Ichia, I. Willner, *Chem. Commun.* **1998**, 1393.

[7] a) P. V. Kamat, S. Barazzouk, S. Hotchandani, *Angew. Chem. Int. Ed.* **2002**, *41*, 2764; b) R. Baron, C. Huang, D. M. Bassani, A. Onopriyenko, M. Zayats, I. Willner, *Angew. Chem.* **2005**, *117*, 4078; c) R. Baron, C. Huang, D. M. Bassani, A. Onopriyenko, M. Zayats, I. Willner, *Angew. Chem. Int. Ed.* **2005**, *44*, 4010.

[8] K. Hata, H. Fujihara, *Chem. Commun.* **2002**, 2714.

[9] a) I. Willner, F. Patolsky, J. Wasserman, *Angew. Chem.* **2001**, *113*, 1913; b) I. Willner, F. Patolsky, J. Wasserman, *Angew. Chem. Int. Ed.* **2001**, *40*, 1861.

[10] W. Zeng, Y. Cao, Y. Bai, Y. Wang, Y. Shi, M. Zhang, F. Wang, C. Pan, P. Wang, *Chem. Mater.* **2010**, *22*, 1915.

[11] a) T. Higashino, H. Imahori, *Dalton Trans.* **2015**, *44*, 448; b) K. Ladomenou, T. N. Kitsopoulos, G. D. Sharma,

A. G. Coutsolelos, *RSC Adv.* **2014**, *4*, 21379; c) B. E. Harbin, H. J. Snaith, M. D. McGhee, *Nat. Photonics* **2012**, *6*, 162; d) H. Imahori, S. Hayashi, T. Umeyama, S. Eu, A. Oguro, S. Kang, Y. Matano, T. Shishido, S. Ngamsinlapasathian, S. Yoshikawa, *Langmuir* **2006**, *22*, 11405; e) W. M. Campbell, A. K. Burrell, D. L. Officer, K. W. Jolley, *Coord. Chem. Rev.* **2004**, *248*, 1363; f) G. De la Torre, C. G. Claessens, T. Torres, *Chem. Commun.* **2007**, 2000.

[12] a) S. Eu, S. Hayashi, T. Umeyama, A. Oguro, M. Kawasaki, N. Kadota, Y. Matano, H. Imahori, *J. Phys. Chem. C* **2007**, *111*, 3528; b) H. Imahorni, T. Umeyama, S. Ito, *Acc. Chem. Res.* **2009**, *42*, 1809; c) L.-L. Li, E. W.-G. Diau, *Chem. Soc. Rev.* **2013**, *42*, 291; d) T. Bessho, S. M. Zakeerubbin, C.-Y. Diau, M. Grätzel, *Angew. Chem.* **2010**, *122*, 6796; e) T. Bessho, S. M. Zakeerubbin, C.-Y. Diau, M. Grätzel, *Angew. Chem. Int. Ed.* **2010**, *49*, 6646.

[13] a) E. Hao, B. Yang, J. Zhang, X. Zhang, J. Sun, J. Shen, *J. Mater. Chem.* **1999**, *8*, 1327; b) P. Yu, K. Zhu, A. G. Norman, S. Ferrere, A. J. Frank, A. J. Nozik, *J. Phys. Chem. B* **2006**, *110*, 25455; c) Y. Tian, T. Newton, N. A. Kotov, D. M. Guldi, J. H. Fendler, *J. Phys. Chem.* **1996**, *100*, 8927; d) I. Bedja, P. V. Kamat, *J. Phys. Chem.* **1995**, *99*, 9182; e) K. Rajeshwar, N. R. de Tacconi, C. R. Chenthamarakshan, *Chem. Mater.* **2001**, *13*, 2765.

[14] a) I. Robel, B. Bunker, P. V. Kamat, *Adv. Mater.* **2005**, *17*, 2458; b) L. Sheeney-Haj-Ichia, B. Basnar, I. Willner, *Angew. Chem.* **2004**, *117*, 80; c) L. Sheeney-Haj-Ichia, B. Basnar, I. Willner, *Angew. Chem. Int. Ed.* **2005**, *44*, 78.

[15] a) C. W. Tang, *Appl. Phys. Lett.* **1986**, *48*, 183; b) A. J. Heeger, *J. Phys. Chem. B* **2001**, *105*, 8475; c) A. J. Breeze, Z. Schlesinger, S. A. Carter, P. J. Brock, *Phys. Rev. B* **2001**, *64*, 125205; d) H. Hoppe, N. S. Sariciftci, *J. Mater. Res.* **2004**, *19*, 1924; e) W. U. Huynh, J. J. Dittmer, A. P. Alivisatos, *Science* **2002**, *295*, 2425.

[16] a) E. Granot, F. Patolsky, I. Willner, *J. Phys. Chem. B* **2004**, *108*, 5875; b) R. Tel-Vered, H. B. Yildiz, I. Willner, *Adv. Mater.* **2009**, *21*, 716.

[17] a) F. D'Souza, O. Ito, *Coord. Chem. Rev* **2005**, *249*, 1410; b) Y. Shi, I. Sanchez-Molina, C. Cao, T. R. Cook, P. J. Stang, *Proc. Natl. Acad. Sci. USA* **2014**, *111*, 9390; c) C. B. Kc, K. Ohkubo, P. A. Karr, S. Fukuzumi, F. D'Souza, *Chem. Commun.* **2013**, *49*, 7614; d) M. Urbani, S. Osati, S. Kuhri, D. M. Guldi, T. Torres, *J. Porphyrins Phthalocyanines* **2013**, *17*, 501; e) A. S. D. Sandanayaka, N. K. Subbaiyan, S. K. Das, R. Chitta, E. Maligaspe, T. Hasobe, O. Ito, F. D'Souza, *ChemPhysChem* **2011**, *12*, 2266; f) F. D'Souza, E. Maligaspe, A. S. D. Sandanayaka, N. K. Subbaiyan, P. A. Karr, T. Hasobe, O. Ito, *J. Phys. Chem. A* **2010**, *114*, 10951.

[18] a) K. Haupt, *Analyst* **2001**, *126*, 747; b) K. Haupt, K. Mosbach, *Chem. Rev.* **2000**, *100*, 2495; c) G. Wulff, *Chem. Rev.* **2002**, *102*, 1; d) M. J. Whitcombe, N. Kirsch, I. A. Nicholls, *J. Mol. Recognit.* **2014**, *27*, 297; e) L. Chen, S. Xu, J. Li, *Chem. Soc. Rev.* **2011**, *40*, 2922; f) F. Dickert, *Anal. Bioanal. Chem.* **2007**, *389*, 353.

[19] a) M. Riskin, R. Tel-Vered, T. Bourenko, E. Granot, I. Willner, *J. Am. Chem. Soc.* **2008**, *130*, 9726; b) M. Riskin, R. Tel-Vered, O. Lioubashevski, I. Willner, *J. Am. Chem. Soc.* **2009**, *131*, 7368; c) M. Riskin, R. Tel-Vered, I. Willner, *Adv. Mater.* **2010**, *22*, 1387; d) M. Riskin, Y. Ben-Amram, R. Tel-Vered, V. Chegel, J. Almog, I. Willner, *Anal. Chem.* **2011**, *83*, 3082.

[20] Y. Ben-Amram, M. Riskin, I. Willner, *Analyst* **2010**, *135*, 2952.

[21] M. Riskin, R. Tel-Vered, M. Frasconi, N. Yavo, I. Willner, *Chem. Eur. J.* **2010**, *16*, 7114.

[22] M. Frasconi, R. Tel-Vered, M. Riskin, I. Willner, *Anal. Chem.* **2010**, *82*, 2512.

[23] Y. Ben-Amram, R. Tel-Vered, M. Riskin, Z. Wang, I. Willner, *Chem. Sci.* **2012**, *3*, 162.

[24] a) M. Frasconi, R. Tel-Vered, J. Elbaz, I. Willner, *J. Am. Chem. Soc.* **2010**, *132*, 2029; b) M. Frasconi, R. Tel-Vered, M. Riskin, I. Willner, *J. Am. Chem. Soc.* **2010**, *132*, 9373.

[25] a) D. Balogh, R. Tel-Vered, M. Riskin, R. Orbach, I. Willner, *ACS Nano* **2011**, *5*, 299; b) D. Balogh, R. Tel-Vered, R. Freeman, I. Willner, *J. Am. Chem. Soc.* **2011**, *133*, 6533.

[26] a) O. Yehezkeli, O. I. Wilner, R. Tel-Vered, D. Roizman-Sade, R. Nechustai, I. Willner, *J. Phys. Chem. B* **2010**, *114*, 14383; b) O. Yehezkeli, R. Tel-Vered, J. Wasserman, A. Trifonov, D. Michaeli, R. Nechushtai, I. Willner, *Nat. Commun.* **2012**, *3*, 742.

[27] a) J. Kuebel, R. Schroot, M. Waechtler, U. S. Schubert, B. Dietzek, M. Jaeger, *J. Phys. Chem. C* **2015**, *119*, 4742; b) J. Hankache, O. S. Wenger, *PhysChemChemPhys* **2012**, *14*, 2685; c) P. P. Laine, S. Campagna, F. Loiseau, *Coord. Chem. Rev.* **2008**, *252*, 2552; d) P. P. Laine, F. Bedioui, F. Loiseau, C. Chiorboli, S. Campagna, *J. Am. Chem. Soc.* **2006**, *128*, 7510; e) M. Lahav, T. Gabriel, A. N. Shipway, I. Willner, *J. Am. Chem. Soc.* **1999**, *121*, 258; f) M. Lahav, V. Heleg-Shabtai, J. Wasserman, E. Katz, I. Willner, H. Dürr, Y.-Z. Hu, S. H. Bossmann, *J. Am. Chem. Soc.* **2000**, *122*, 11480.

[28] a) J. Hankache, M. Niemi, H. Lemmetyinen, O. S. Wenger, *J. Phys. Chem. A* **2012**, *116*, 8159; b) J. Hankache, M. Niemi, H. Lemmetyinen, O. S. Wenger, *Inorg. Chem.* **2012**, *51*, 6333; c) J. H. Si, Y. G. Wang, Q. G. Yang, P. X. Ye, H. J. Tian, Q. F. Zhou, H. J. Xu, *Appl. Phys. B* **1997**, *64*, 663.

[29] a) A. Song, H. Zhang, M. Zhang, T. Shen, *Dyes Pigm.* **1999**, *42*, 149; b) L. Huang, X. Cui, B. Therrien, J. Zhao, *Chem. Eur. J.* **2013**, *19*, 17472.

[30] a) R. J. Kumar, S. Karlsson, D. Streich, A. Rolandini Jensen, M. Jaeger, H. Becker, J. Bergquist, O. Johansson, L. Hammarstroem, *Chem. Eur. J.* **2010**, *16*, 2830; b) J. P. Collin, S. Guillerez, J. P. Sauvage, F. Barigelletti, L. De Cola, L. Flamigni, V. Balzani, *Inorg. Chem.* **1992**, *31*, 4112; c) J. P. Collin, S. Guillerez, J. P. Sauvage, F. Barigelletti, L. Flamigni, L. De Cola, V. Balzani, *Coord. Chem. Rev.* **1991**, *111*, 291.